Codebook-Based IRS System: Impact of Channel Estimation Errors and Pilot Power Adaptation on Codeword Selection and Data Rate

Sriram Ganesan, Neelesh B. Mehta, *Fellow, IEEE*, and Rimalapudi Sarvendranath, *Member, IEEE*

***Abstract*— The codebook-based scheme for intelligent reflecting surfaces (IRSs) decouples the training and control signaling overheads from the number of IRS elements by selecting the IRS reflection pattern from a pre-specified codebook. We analyze the performance of a training scheme that exploits a novel trade-off between the powers allocated for selection pilots, which are used to select the reflection pattern, and the demodulation pilot, which is used for estimating the channel for demodulation. We develop a selection-aware linear minimum mean-square error estimator of the effective channel gain of the selected reflection pattern. When the direct link is blocked, we derive an elegant closed-form expression for the beamforming gain. When the direct link is present, which requires a different analysis, we derive a novel upper bound and insightful asymptotic expressions for the beamforming gain. We then present a novel expression for the achievable rate that accounts for the impact of noisy channel estimates on both selection of the reflection pattern and demodulation of data. We optimize the pilot and data powers and the codebook size. Our approach yields a significantly better rate than conventional schemes, and establishes the advantages of allocating substantially different powers to the selection and demodulation pilots and data.**

***Index Terms*— IRS, codebook-based training, selection, pilots, channel estimation, power allocation, rate.**

I. Introduction

AN INTELLIGENT reflecting surface (IRS) is made up of a large number of low-cost passive elements. Each of the reflective elements can induce a programmable phase-shift to the incident electromagnetic signal, which enables the system designer to program the radio propagation environment. For example, in passive beamforming, the phase-shifts of these passive elements can be configured to form a beam in the desired direction without requiring a radio frequency chain with a power amplifier [2]. IRS improves energy-efficiency compared to the conventional relay and massive multiple-input multiple-output (MIMO) systems. It improves coverage in areas where the direct link between the access point (AP) and the user is blocked. Further, it can tackle both large-scale fading and small-scale fading effects. This makes IRS an appealing candidate technology for 6G.

Configuring the reflection coefficient at each IRS element, which depends on the channel gains, is crucial to realize the above benefits. However, a passive IRS with no signal processing capabilities cannot estimate these channel gains and, thereafter, configure the IRS. Hence, cascaded channel estimation plays a crucial role in an IRS-aided system and has recently spurred a lot of research [3], [4], [5], [6]. Three different ways of configuring IRS reflection coefficients have been considered in the literature, namely, instantaneous channel state information (CSI) based, statistical-CSI-based, and codebook-based. We summarize and contrast them below.

a) Instantaneous-CSI-Based Schemes: In the classical on-off scheme, only one element is configured to be in the reflection mode when a pilot is transmitted [3], [4]. Instead, in the discrete Fourier transform (DFT)-based scheme, all the IRS elements are configured to be in the reflection mode and different columns of the DFT matrix are used as reflection patterns for different pilot transmissions [5]. Thus, in estimation-based schemes, each of the M cascaded channel gains is estimated, where M is the number of IRS elements. Based on these estimates, the AP determines the reflection pattern and communicates it to the IRS via a control link. This requires a pilot overhead of $\mathcal{O}(M)$ and a control overhead of $\mathcal{O}(M)$. Thus, these schemes entail large pilot and control overheads.

Extensions and variations of these schemes have been studied in [4], [5], [7], [8], and [9]. IRS element grouping is proposed in [6] to reduce the pilot overhead. The sparsity of the AP-IRS channel in the spatial domain is exploited in [3], [10], and [11] to reduce the pilot overhead. Machine-learning-based approaches are instead pursued in [12], [13], [14], and [15]. Pairwise error probability and asymptotic average bit error probability expressions are derived in [16] for an IRS-assisted space-shift keying system with channel estimation errors.

b) Statistical-CSI-Based Schemes: In statistics-based schemes, the IRS configuration is based on channel statistics such

Received 9 March 2024; revised 20 June 2024 and 22 August 2024; accepted 22 October 2024. Date of publication 6 November 2024; date of current version 12 December 2024. This work was supported by the J. C. Bose Fellowship under Grant JCB/2023/000028. The work of Rimalapudi Sarvendranath was supported in part by the Science and Engineering Research Board (SERB) under Grant SRG/2023/000070 and in part by the Department of Science and Technology (DST) Innovation in Science Pursuit for Inspired Research (INSPIRE) Research Grant. An earlier version of this paper was presented in part at IEEE ICASSP, Seoul, South Korea, April 2024 [DOI: 10.1109/ICASSP48485.2024.10445981]. The associate editor coordinating the review of this article and approving it for publication was Y. Zhu. *(Corresponding author: Neelesh B. Mehta.)*

Sriram Ganesan and Neelesh B. Mehta are with the Department of Electrical Communication Engineering, Indian Institute of Science (IISc), Bengaluru 560012, India (e-mail: sriramgsuccess@gmail.com; nbmehta@iisc.ac.in).

Rimalapudi Sarvendranath is with the Department of Electrical Engineering, Indian Institute of Technology (IIT) Tirupati, Tirupati 517619, India (e-mail: sarvendranath@iittp.ac.in).

Color versions of one or more figures in this article are available at https://doi.org/10.1109/TWC.2024.3488189.

Digital Object Identifier 10.1109/TWC.2024.3488189

1536-1276 © 2024 IEEE. Personal use is permitted, but republication/redistribution requires IEEE permission.
See https://www.ieee.org/publications/rights/index.html for more information.

Authorized licensed use limited to: Indian Institute of Technology. Downloaded on February 05,2025 at 11:59:49 UTC from IEEE Xplore. Restrictions apply.

TABLE I
COMPARISON WITH LITERATURE ON CODEBOOK-BASED SCHEMES

Reference	Impact of noise on selection	Impact of noise on demodulation	Pilot and data powers	Analysis with estimation errors	Duplexing
[12]	No	No	Not optimized	No	TDD
[20]	Yes	No	Not optimized	Loose bounds	TDD
[21]	Yes	No	Not optimized	No	TDD
[22]	Yes	No	Not optimized	No	TDD
Our manuscript	Yes	Yes	Optimized	Yes (With and without direct link)	TDD/FDD

as covariance [17], [18], [19]. It is not a function of the instantaneous cascaded channel gains. Since the channel statistics vary slowly, the training overhead, when amortized over time, is lower. However, the beamforming gain is also lower.

c) Codebook-Based Schemes: In codebook-based schemes, one of the reflection patterns that optimizes a selection metric is selected from a pre-designed codebook with $K < M$ reflection patterns and is configured at the IRS during data transmission [20], [21], [22], [23], [24], [25]. The codebook-based scheme is practically appealing due to its lower pilot and signaling overheads. It needs K pilots to select the reflection pattern and only $\lceil \log_2(K) \rceil$ bits, where $\lceil . \rceil$ denotes the ceiling function, to send the reflection pattern index to the IRS. This is much lower than that of the instantaneous-CSI-based schemes and enables the system designer to control the overhead. We, therefore, focus on these codebook-based schemes and explore the trade-off between the training overhead and the beamforming gain, and its implications on the data rate.

A two-phase protocol for the codebook-based scheme is studied in [20] and [21]. In the first phase, for each codebook vector, the user transmits pilots in the uplink to enable the AP to select the codebook vector that yields the largest signal-to-noise ratio (SNR). In the second phase, assuming reciprocity, the IRS configures the selected reflection pattern and the AP transmits downlink data. For this protocol, [21] derived the beamforming gain for a random codebook, assuming perfect channel state information and no direct link. Reference [20] derived an upper bound on the beamforming gain for the random and equi-partition codebooks considering imperfect CSI and a direct link. A codebook that incorporates user position information is considered in [22], but the achievable rate is studied only through simulations. For the DFT matrix-based codebook, a deep learning model is developed to select the codebook vector that maximizes the achievable rate in [12]. Codebook-based schemes for surfaces that can reflect and refract simultaneously are studied in [24] and [25].

A. Focus and Contributions

We present a comprehensive analysis of a codebook-based IRS-assisted communication system in the presence of noisy channel estimates, which are inevitable in practice due to finite pilot powers. They affect the codebook-based scheme in two ways. First, they can cause a sub-optimal reflection pattern to be selected. Second, this sub-optimal pattern together with the noisy estimate of the effective channel affect demodulation and lower the data rate. Table I compares our work with the literature on codebook-based schemes. As shown in the table, the impact of noisy channel estimates on demodulation has not been studied in the literature even though it is a general problem in codebook-based IRS systems.

We make the following contributions. First, we propose a training scheme that separates the tasks of selection of the reflection pattern and demodulation. In it, the AP first sends K selection pilots to the user, one for each codeword available in the codebook. Therefore, the minimum number of selection pilots required is K. The user selects the reflection pattern with the highest received signal strength and feeds back its index to the AP. The AP subsequently forwards it to the IRS. The AP then sends a demodulation pilot to enable the user to obtain a better estimate of the effective channel gain to demodulate the data symbols that follow. One advantage of this scheme is that more power can be allocated to just the demodulation pilot to obtain an accurate estimate of the effective channel gain required for coherent demodulation. In the absence of this demodulation pilot, the AP would need to allocate sufficiently high power to each of the selection pilots as it does not a priori know which codeword will be selected.

Second, our training scheme does not require channel reciprocity because the AP transmits all the pilots and the UE only feeds back the index of the selected codeword. Thus, our scheme applies to both time-division duplex (TDD) and frequency-division duplex (FDD) systems. This is unlike [20], [21], [22], where UE transmits pilots in uplink and AP selects the codeword to transmit data in downlink. This requires reciprocity and works only for TDD. Third, our analysis tackles noisy estimates and the correlation among the signals received from different reflection patterns due to the presence of the common direct link. This correlation makes the analysis considerably more involved.

Lastly, for a given total pilot plus data power budget, we show that a novel trade-off exists between the powers allocated to the selection pilot, the demodulation pilot, and the data symbols. Allocating more power to the selection pilots improves the odds that the optimal reflection pattern is selected. However, it reduces the power available for the demodulation pilot and the data, which can lower the data rate. Allocating more power to the demodulation pilot improves the accuracy of the channel estimate used for demodulation. However, this again reduces the power available for data and can lower the data rate. Exploiting this trade-off and allocating optimal powers to the pilots and the data symbols improves the rate compared to the conventional approaches. To the best of our knowledge, none of the works on codebook-based schemes have optimized the allocation of powers between the pilot(s) and the data [24], [26], [27], [28].

Authorized licensed use limited to: Indian Institute of Technology. Downloaded on February 05,2025 at 11:59:49 UTC from IEEE Xplore. Restrictions apply.

For the proposed training scheme, we make the following contributions:

- *Beamforming Gain Analysis with Imperfect CSI:* When the direct link is blocked, we derive closed-form expressions for the probability density function (PDF) of the channel gain of the selected reflection pattern and the beamforming gain of the IRS. The significance and novelty of this analysis lies in its accounting for the impact of imperfect CSI on the selection of the reflection pattern as well as coherent demodulation. The analysis applies to the general class of orthogonal codebooks, which includes the DFT and Hadamard matrix-based codebooks [12]. When the direct link is present, we derive a novel upper bound on the beamforming gain. This is different from the bound derived in [20], which becomes unacceptably loose as the number of IRS elements increases and applies only to random codebooks. Our analysis handles imperfect CSI and the correlation due to presence of the direct link. It develops an alternate virtual selection criterion for the reflection pattern and employs novel arguments to show that its beamforming gain upper bounds that of the proposed scheme.
- *Rate Analysis and Optimal Power Allocation with Imperfect CSI:* We first derive a novel selection-aware linear minimum mean-square error (LMMSE) estimator of the effective channel gain. It exploits the fact that the statistics of the effective channel gain of the selected pattern differ from those of an arbitrary pattern. Using this estimator, we derive an expression for the achievable rate that accounts for the training, feedback, and control signaling overheads of the codebook-based scheme. We then numerically determine the optimal selection and demodulation pilot powers and data power that maximize the achievable rate subject to a total power constraint. Only the asymptotic beamforming gain for a large number of IRS elements is analyzed in [21]. Furthermore, this is done assuming perfect CSI, a random codebook, and the absence of a direct link. While the direct link is considered in [22], the achievable rate is evaluated only through simulations.
- *Novel Insights:* For low and high SNR regimes, we use recent results from extreme value theory to derive insightful closed-form expressions of the beamforming gain with and without the direct link. The expressions bring out role of the number of reflection patterns, the coherence interval, the number of IRS elements, and the total power available at the AP. We show that the beamforming gain increases linearly with the number of IRS elements but logarithmically with the codebook size.
- *Numerical Results:* We study the trade-off between the codebook size, which also affects the training overhead, and the achievable rate. The proposed scheme achieves a higher rate than the conventional codebook-based and estimation-based schemes in regimes of practical interest. This is due to its low training overhead and ability to allocate significantly higher power to the demodulation pilot than a selection pilot. These gains persist even when the cascaded channel gains are correlated.

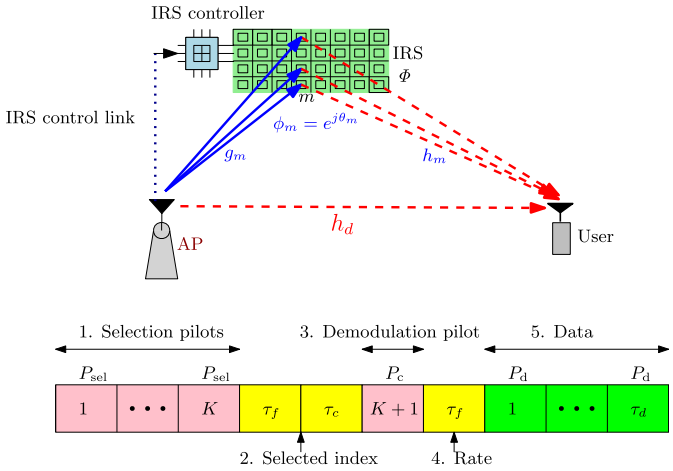


Fig. 1. System model showing an IRS with M reflecting elements. Also shown is the proposed training and data transmission scheme.

B. Outline and Notations

The system model and the proposed transmission scheme are described in Section II. Section III formulates the optimization problem and solves it when the direct link is blocked. Section IV addresses the case where both direct and reflected links are present. Numerical results are presented in Section V. Our conclusions follow in Section VI.

Notation: We show scalar variables in normal, vector variables in lowercase bold, matrices in uppercase bold, and sets in calligraphic fonts. We denote the probability of an event B by $\Pr(B)$ and the probability of B conditioned on an event A by $\Pr(B \mid A)$. For a complex number u, $\Re\{u\}$, $\Im\{u\}$, u^*, and $|u|$ denote its real part, imaginary part, complex conjugate, and absolute value, respectively. $\mathbb{E}[.]$ denotes expectation. The expectation over a random variable (RV) X is denoted by $\mathbb{E}_X[.]$ and the expectation over X conditioned on the RV Y by $\mathbb{E}_{X|Y}[.]$. The notation $\mathbf{X} \sim \mathcal{CN}(\boldsymbol{\mu}, \mathbf{C})$ means that $\mathbf{X}$ is a complex normal random vector with mean $\boldsymbol{\mu}$ and covariance $\mathbf{C}$. We denote the $M \times M$ identity matrix by $\mathbf{I}_M$ and the transpose operation by $(.)^T$. The indicator function is denoted by $\mathbb{1}_{\{a\}}$, which equals one if a is true and is zero otherwise.

II. System Model and Proposed Transmission Scheme

In the system model illustrated in Figure 1, the AP transmits data to a user with the help of an IRS with M reflecting elements. Let h_d denote the direct channel gain between the AP and the user. Let g_m denote the channel gain between the AP and the m^{th} IRS element, and h_m denote the channel gain between the m^{th} IRS element and the user. Let $\mathbf{g} = [g_1, g_2, \ldots, g_M]^T$ and $\mathbf{h} = [h_1, h_2, \ldots, h_M]^T$.

Channel Model: We consider a quasi-static, flat-fading channel model. We assume a strong line-of-sight (LoS) path between the AP and the IRS, which is practically justified when the AP is placed on a rooftop and the IRS on the outside of a wall. Hence, $\mathbf{g}$ is a deterministic LoS channel gain vector [7], [20]. The direct and IRS-user links undergo Rayleigh fading. Therefore, $h_d \sim \mathcal{CN}(0, \beta_d)$ and $\mathbf{h} \sim \mathcal{CN}(\mathbf{0}, \beta_h \mathbf{I}_M)$,

Authorized licensed use limited to: Indian Institute of Technology. Downloaded on February 05,2025 at 11:59:49 UTC from IEEE Xplore. Restrictions apply.

where β_d and β_h are the path-losses of the direct and IRS-user links, respectively. The direct link channel gain h_d is independent of $\mathbf{h}$. Let β_g denote the path-loss of the AP-IRS link.

Let $\boldsymbol{\phi} = [\phi_1, \phi_2, \ldots, \phi_M]^T$ denote the reflection pattern for the IRS elements, where $\phi_m = e^{j\theta_m}$ is the reflection coefficient and $\theta_m \in [0, 2\pi]$ is the phase-shift of the m^{th} reflecting element. When the reflection pattern $\boldsymbol{\phi}$ is configured at the IRS, the signal y received at the user is given by [2]

$$y = \left(h_d + \sum_{m=1}^{M} h_m \phi_m g_m \right) x + n = \left(h_d + \mathbf{r}^T \boldsymbol{\phi} \right) x + n, \tag{1}$$

where x is the transmitted signal, $n \sim \mathcal{CN}(0, \sigma^2)$ is additive white Gaussian noise (AWGN), and $\mathbf{r} = [r_1, r_2, \ldots, r_M]^T = [h_1 g_1, h_2 g_2, \ldots, h_M g_M]^T$ is the cascaded reflected channel gain vector.

Comments: The above model assumes that $h_1, h_2, \ldots, h_M$ are independent and identically distributed (i.i.d.). This makes the analysis tractable, and has also been assumed in [4], [20], and [29]. In Section V, we show the efficacy of our approach in the presence of correlation between the cascaded channel gains and imperfect CSI. We consider a single-antenna AP and user. We note that a rigorous analysis and rate optimization that considers the cumulative impact of channel estimation errors on the beamforming gain and rate of codebook-based training is not available in the literature even for the independent channel gains model with a single antenna at the AP and the user.

A. Proposed Training and Transmission Scheme

A codebook consisting of $K \leq M$ orthogonal reflection patterns $\boldsymbol{\phi}(1), \boldsymbol{\phi}(2), \ldots, \boldsymbol{\phi}(K)$ is used for generating the reflection coefficients at the IRS. This model includes the DFT and Hadamard codebooks considered in the literature [5]. The training and transmission scheme consists of the following phases:

1) *Selection Phase:* To enable the user to select the reflection pattern that maximizes the rate, the AP sequentially transmits K *selection pilot* symbols, each with power P_{sel}. Note that the number of pilot symbols is equal to the size of the codebook. The reflection pattern $\boldsymbol{\phi}(i)$ is configured at the IRS when the i^{th} pilot is transmitted. Without loss of generality, the pilot symbols are identical and are given by $p = 1$. The signal y_i received by the user, for $1 \leq i \leq K$, is

$$y_i = \sqrt{P_{\text{sel}}} \left(h_d + \mathbf{r}^T \boldsymbol{\phi}(i) \right) + n_i = \sqrt{P_{\text{sel}}} h_{eq}(i) + n_i. \tag{2}$$

Here, $n_1, n_2, \ldots, n_K \sim \mathcal{CN}(0, \sigma^2)$ are i.i.d. AWGN, and

$$h_{eq}(i) = h_d + \mathbf{r}^T \boldsymbol{\phi}(i), \tag{3}$$

is the effective AP-user channel gain. The user selects the reflection pattern $\boldsymbol{\phi}(s)$ with the largest received signal strength. Hence,

$$s = \text{argmax}_{i \in \{1,2,\ldots,K\}} \{|y_i|^2\}. \tag{4}$$

2) *Feedback and Control Signaling Phase:* The user feeds back the selected index s to the AP. This incurs a feedback overhead of $\lceil \log_2(K) \rceil$ bits and requires a time duration of τ_f. The AP then sends s to the IRS via a control link and the IRS configures $\boldsymbol{\phi}(s)$ as the reflection pattern. This incurs a control overhead of $\lceil \log_2(K) \rceil$ bits and requires a time duration of τ_c. We assume that the feedback error probability is negligible. This can be ensured by protecting the feedback bits using error correcting codes. Furthermore, a pilot symbol can be sent along with the feedback bits to enable the AP to demodulate the fed back bits.
3) *Estimation Phase:* The AP sends a *demodulation pilot* $p = 1$ with power P_c to enable the user to accurately estimate the effective channel gain $h_{eq}(s)$ for coherent demodulation. The signal y_c at the user is

$$y_c = \sqrt{P_c} h_{eq}(s) + n_c, \tag{5}$$

where $n_c \sim \mathcal{CN}(0, \sigma^2)$ is AWGN. Intuitively, $h_{eq}(s)$ can be accurately estimated by increasing the power of just one demodulation pilot instead of the powers of all K selection pilots.
4) *Feedback of Rate:* Based on its estimate of $h_{eq}(s)$, the user feeds back to the AP the data rate R with which it can receive data. This requires a time duration of τ_f. We derive the expression for R below.
5) *Data Transmission Phase:* The AP sends τ_d downlink data symbols to the user, each with power P_d. The symbols are encoded with rate R. The signal y_d received at the user when the data symbol x is transmitted is given by

$$y_d = \sqrt{P_d} h_{eq}(s) x + n_d, \tag{6}$$

where $n_d \sim \mathcal{CN}(0, \sigma^2)$ is AWGN.

Next, we analyze the performance of the above protocol for the scenarios without and with the direct link in Sections III and IV, respectively. The analytical tools required and the technical nature of the results turn out to be different for these two scenarios.

III. Analysis: Without Direct Link

In this section, we consider the case where the direct link between the AP and the user is blocked due to obstacles [2], [24]. Hence, $h_{eq}(i) = \mathbf{r}^T \boldsymbol{\phi}(i)$. We first develop a reflection pattern selection-aware LMMSE estimator for the effective channel gain. Its novelty lies in exploiting the ordered-statistics of the received signal strength of the selected codeword. Using this, we derive a bound on the achievable rate. We then determine the optimal pilot and data power allocation that maximizes the rate.

Authorized licensed use limited to: Indian Institute of Technology. Downloaded on February 05,2025 at 11:59:49 UTC from IEEE Xplore. Restrictions apply.

A. Selection-Aware LMMSE Estimator for $h_{eq}(s)$

The LMMSE estimate $\hat{h}_{eq}(s)$ of the effective channel gain $h_{eq}(s)$ is given by [30, Ch. 12][1]

$$\hat{h}_{eq}(s) = a y_c + b, \tag{7}$$

where

$$a = \frac{\mathrm{Cov}\left(y_c, h_{eq}(s)\right)}{\mathrm{Var}\left(y_c\right)}, \tag{8}$$

$$b = \left(1 - \sqrt{P_c} a\right) \mathbb{E}\left[h_{eq}(s)\right]. \tag{9}$$

$\mathrm{Cov}\left(y_c, h_{eq}(s)\right)$ is the covariance of y_c and $h_{eq}(s)$, and $\mathrm{Var}\left(y_c\right)$ is the variance of y_c. A key point to note is that $h_{eq}(s)$ does not follow the same statistics as $h_{eq}(1), h_{eq}(2), \ldots, h_{eq}(K)$ due to the selection of the IRS reflection pattern based on (4). We derive its statistics below. For this, we first state a useful lemma about the independence of $h_{eq}(1), h_{eq}(2), \ldots, h_{eq}(K)$.

Lemma 1: The effective channel gains $h_{eq}(1), h_{eq}(2), \ldots, h_{eq}(K)$ are i.i.d. complex normal RVs with mean 0 and variance $M\beta_g\beta_h$.

Proof: The proof is given in Appendix A. ∎

Let $\beta_r = M\beta_g\beta_h$ denote the effective average channel strength of the reflected link and $\sigma_y^2 = P_{\text{sel}}\beta_r + \sigma^2$ denote the variance of signal y_i received during the selection phase. We now derive the PDF of $h_{eq}(s) = e_{rs} + j e_{is}$, where e_{rs} and e_{is} denote its real and imaginary parts, respectively, in closed-form.

Theorem 1: The PDF $f_{e_{rs},e_{is}}(x,z)$ of the complex RV $h_{eq}(s)$, where $x, z \in \mathbb{R}$, is given by

$$f_{e_{rs},e_{is}}(x,z) = \frac{K\sigma_y^2}{\pi\beta_r} \sum_{l=0}^{K-1} \binom{K-1}{l} \frac{(-1)^l}{\sigma_y^2 + l\sigma^2} \times \exp\left(\frac{-(l+1)\sigma_y^2}{\left(\sigma_y^2 + l\sigma^2\right)\beta_r}\left(x^2 + z^2\right)\right). \tag{10}$$

Proof: The proof is given in Appendix B. ∎

The symmetric form of the PDF in (10) implies $\mathbb{E}\left[h_{eq}(s)\right] = 0$, which, in turn, yields $b = 0$. We can also show from (5) and (8) that $a = \sqrt{P_c}\,\mathbb{E}\left[\left|h_{eq}(s)\right|^2\right] \Big/ \left(P_c\,\mathbb{E}\left[\left|h_{eq}(s)\right|^2\right] + \sigma^2\right)$. Thus, from (7), we get

$$\hat{h}_{eq}(s) = \frac{\sqrt{P_c}\,\mathbb{E}\left[\left|h_{eq}(s)\right|^2\right]}{P_c\,\mathbb{E}\left[\left|h_{eq}(s)\right|^2\right] + \sigma^2} y_c. \tag{11}$$

The PDF derived in Theorem 1 leads to the following insightful closed-form expression for the beamforming gain $B_{\text{g}} = \mathbb{E}\left[\left|h_{eq}(s)\right|^2\right]$ of the codebook-based scheme.

Corollary 1: The beamforming gain B_{g} in the presence of channel estimation errors is given by

$$B_{\text{g}} = \frac{\beta_r\left(P_{\text{sel}}\beta_r\left[\psi(K+1) + \gamma\right] + \sigma^2\right)}{P_{\text{sel}}\beta_r + \sigma^2}, \tag{12}$$

where $\psi(.)$ is the digamma function [31, Ch. 6] and $\gamma \approx 0.577$ is the Euler-Mascheroni constant [31, Ch. 6].

Proof: The proof is given in Appendix C. ∎

The impact of P_{sel} and K on the beamforming gain is brought out by the next corollary. Substituting this expression in (11) yields the LMMSE estimator. The selection-unaware estimator, which is based on unordered statistics, would be $\hat{h}_{eq}(s) = \sqrt{P_c}\beta_r y_c / \left(P_c\beta_r + \sigma^2\right)$. It is different from the selection-aware estimator.

Corollary 2: B_{g} is a concave, monotonically increasing function of P_{sel} for $K > 1$ and is a concave, monotonically increasing function of K for $K \geq 1$.

Proof: The proof is given in Appendix D. ∎

Thus, increasing P_{sel} or K leads to a diminishing increase in the beamforming gain. Since $\psi(K+1) \approx \log(K+1) - \left(1/\left(K+1\right)\right)$ and $\beta_r = M\beta_g\beta_h$, it follows that B_{g} increases logarithmically with K and linearly with M.

B. Achievable Rate With Noisy Channel Estimates

The achievable rate R in the presence of channel estimation errors is given by [32][2]

$$R = \frac{\tau_d}{T_{\text{c}}}\,\mathbb{E}\left[\log_2\left(1 + \frac{P_d\left|\hat{h}_{eq}(s)\right|^2}{\sigma^2 + P_d\sigma^2_{\hat{h}_{eq}(s)}}\right)\right], \tag{13}$$

where $\sigma^2_{\hat{h}_{eq}(s)} = \mathbb{E}\left[\left|h_{eq}(s) - \hat{h}_{eq}(s)\right|^2\right]$ is the MSE of the estimate of $h_{eq}(s)$ and $T_{\text{c}} = \tau_d + K + 1 + 2\tau_f + \tau_c$ is the number of symbols in a coherence time interval. T_{c} accounts for the pilot, feedback, and control signaling overheads. Using the Jensen's inequality, we get the following bound:

$$R \leq \frac{\tau_d}{T_{\text{c}}}\log_2\left(1 + \frac{P_d\,\mathbb{E}\left[\left|\hat{h}_{eq}(s)\right|^2\right]}{\sigma^2 + P_d\sigma^2_{\hat{h}_{eq}(s)}}\right). \tag{14}$$

We shall see in Section V that the bound is tight even for small M. This is because the multiple IRS elements reduce the random fluctuations and lead to channel hardening [33].

From (11), $\mathbb{E}\left[\left|\hat{h}_{eq}(s)\right|^2\right]$ can be written as

$$\mathbb{E}\left[\left|\hat{h}_{eq}(s)\right|^2\right] = \frac{P_c\left(B_{\text{g}}\right)^2}{\left(P_cB_{\text{g}} + \sigma^2\right)^2}\,\mathbb{E}\left[\left|y_c\right|^2\right], \tag{15}$$

where $\mathbb{E}\left[\left|y_c\right|^2\right] = P_cB_{\text{g}} + \sigma^2$ since $h_{eq}(s)$ and n_{c} are uncorrelated. Hence,

$$\mathbb{E}\left[\left|\hat{h}_{eq}(s)\right|^2\right] = \frac{P_c\left(B_{\text{g}}\right)^2}{P_cB_{\text{g}} + \sigma^2}. \tag{16}$$

[1]The minimum mean-square error (MMSE) estimator is optimal in terms of minimizing the MSE. However, it is intractable due to the order statistics and the non-Gaussian random variables involved. We, therefore, employ the tractable LMMSE estimator. Furthermore, the two observations y_c and y_s can be used to obtain a more refined channel estimate of $h_{eq}(s)$. However, this approach yields only a marginal gain.

[2]The rate expression is applicable when $\mathbb{E}\left[h_{eq}(s) - \hat{h}_{eq}(s)|\hat{h}_{eq}(s)\right] = 0$ [32]. This holds when $h_{eq}(s)$ is a complex normal RV since $\hat{h}_{eq}(s)$ is an LMMSE estimate of $h_{eq}(s)$. We note that $h_{eq}(s)$ is not a complex normal RV even though $h_{eq}(1), h_{eq}(2), \ldots, h_{eq}(K)$ are complex normal RVs. Therefore, the expression in (13) is an approximation, which makes the problem tractable and leads to valuable insights about the impact of the system parameters on the rate. For smaller K and at lower SNRs, this approximation can be numerically shown to be accurate and the PDF of $h_{eq}(s)$ approaches the complex normal PDF in these regimes. These results are not shown to conserve space.

Authorized licensed use limited to: Indian Institute of Technology. Downloaded on February 05,2025 at 11:59:49 UTC from IEEE Xplore. Restrictions apply.

From (5) and (11), the MSE simplifies to $\sigma^2_{\hat{h}_{eq}(s)} = B_{\mathrm{g}}\sigma^2/\left(P_c B_{\mathrm{g}} + \sigma^2\right)$. Substituting $\sigma^2_{\hat{h}_{eq}(s)}$ and (16) in (14), we get

$$R \leq \frac{\tau_d}{T_{\mathrm{c}}} \log_2 \left(1 + \frac{P_d P_c \left(B_{\mathrm{g}}\right)^2}{\sigma^2 \left[\left(P_d + P_c\right) B_{\mathrm{g}} + \sigma^2\right]}\right). \tag{17}$$

The rate is a function of the demodulation pilot power P_c and the data power P_d. It is also an implicit function of the selection pilot power P_{sel} since B_{g} depends on it.

C. Rate Maximization and Optimal Power Allocation

Our goal is to optimally allocate powers to the pilots and data to maximize the achievable data rate. Given the tractable upper bound in (17), we maximize it instead. Therefore, our problem that optimizes P_{sel}, P_c, and P_d to maximize the upper bound subject to the total power constraint can be written as:

$$\max_{P_{\mathrm{sel}}, P_c, P_d} \left\{\frac{\tau_d}{T_{\mathrm{c}}} \log_2 \left(1 + \frac{P_d P_c \left(B_{\mathrm{g}}\right)^2}{\sigma^2 \left[\left(P_d + P_c\right) B_{\mathrm{g}} + \sigma^2\right]}\right)\right\}, \tag{18}$$

$$\text{s.t.} \quad K P_{\mathrm{sel}} + P_c + \tau_d P_d = P_T, \tag{19}$$

$$P_{\mathrm{sel}} \geq 0, P_c \geq 0, P_d \geq 0. \tag{20}$$

Here, (19) constrains the total power allowed at the AP for transmitting the selection and demodulation pilots and the data to be less than or equal to P_T. Solving the above optimization problem allows us to exploit the trade-off between the pilot and data powers. Due to the monotonically increasing nature of the logarithmic function, maximizing the objective function in (18) is equivalent to maximizing $P_d P_c \left(B_{\mathrm{g}}\right)^2 / \left(\sigma^2 \left[\left(P_d + P_c\right) B_{\mathrm{g}} + \sigma^2\right]\right)$.

No closed-form solution exists for the above optimization problem since the objective is a non-linear function of the variables P_{sel}, P_c, and P_d. Therefore, we obtain the optimal powers numerically. The above expression for the rate enables us to equate the expression for the gradient to 0 and solve for the optimal solution. We substitute $P_d = \left(P_T - K P_{\mathrm{sel}} - P_c\right)/\tau_d$ to obtain the objective function in terms of P_c and P_{sel}. We denote it by $\eta(P_c, P_{\mathrm{sel}})$. It is equal to

$$\eta(P_c, P_{\mathrm{sel}}) = \frac{\left(P_T - K P_{\mathrm{sel}} - P_c\right) P_c \left(B_{\mathrm{g}}\right)^2}{\sigma^2 \left[\left(P_T - K P_{\mathrm{sel}} + (\tau_d - 1) P_c\right) B_{\mathrm{g}} + \tau_d \sigma^2\right]}. \tag{21}$$

Note that B_{g} given in (12) is a function of P_{sel}. Equating the partial derivatives of $\eta(P_c, P_{\mathrm{sel}})$ with respect to P_c and P_{sel} to zero and numerically solving the two equations simultaneously yields the critical points P_c^* and P_{sel}^*. We have found numerically that while multiple critical points can exist, only one of them satisfies the constraints in (20) and is the optimal solution.

D. Asymptotic Results

We now study the asymptotic regimes of small and large selection pilot powers to gain deeper insights about the dependence of the beamforming gain on the system parameters.

1) *When* $(P_{sel}/\sigma^2) \to \infty$*:* We can show that (12) simplifies to

$$B_{\mathrm{g}} \to \beta_r \left[\psi(K+1) + \gamma\right]. \tag{22}$$

This corresponds to a genie-aided (noise-free) selection of the reflection pattern. Thus, the upper bound on R becomes $\frac{\tau_d}{T_{\mathrm{c}}} \log_2 \left(1 + \frac{P_d P_c \beta_r^2 [\psi(K+1)+\gamma]^2}{\sigma^2 [(P_d+P_c)\beta_r [\psi(K+1)+\gamma]+\sigma^2]}\right)$.

2) *When* $(P_{sel}/\sigma^2) \to 0$*:* We can show that (12) simplifies to

$$B_{\mathrm{g}} \to \beta_r. \tag{23}$$

This is equal to the average channel power gain obtained by a random-phase configuration. In this case, the upper bound on R becomes $\frac{\tau_d}{T_{\mathrm{c}}} \log_2 \left(1 + \frac{P_d P_c \beta_r^2}{\sigma^2 [(P_d+P_c)\beta_r + \sigma^2]}\right)$. Since $\psi(K+1) + \gamma > 1$ for $K \geq 2$, it follows that the beamforming gain and rate of the random phase-shift scheme are less than those of the proposed scheme even for small K.

IV. Analysis: With Direct Link

We now consider the case where both direct and reflected links are present. Hence, $h_{eq}(i) = h_d + \mathbf{r}^T \boldsymbol{\phi}(i)$. The common term h_d in the expressions for $h_{eq}(1), h_{eq}(2), \ldots, h_{eq}(K)$ makes them correlated. This makes the analysis of the beamforming gain $B_{\mathrm{g}} = \mathbb{E}\left[|h_{eq}(s)|^2\right]$, the design of the selection-aware estimator, and the rate analysis considerably more challenging.

A. Exact Expression, Asymptotic Insights, and a Bound for B_g

We first present an exact expression for the beamforming gain with the direct link.

Theorem 2: The beamforming gain of the selected reflection pattern is given by

$$\begin{aligned} B_{\mathrm{g}} &= \int_0^\infty \Bigg[1 - \frac{1}{\beta_r \beta_d \sigma^2} \left(\int_0^\infty \int_0^x \int_0^\infty e^{-\frac{u+v}{\beta_r}} e^{-\frac{u}{\beta_d}} \right. \\ &\quad \times I_0\left(\sqrt{\frac{4uv}{\beta_r^2}}\right) I_0\left(\sqrt{\frac{4P_{\mathrm{sel}} vz}{\sigma^4}}\right) e^{\frac{-\left(z + P_{\mathrm{sel}} v\right)}{\sigma^2}} \\ &\quad \left. \times \left(1 - Q_1\left(\frac{\sqrt{2P_{\mathrm{sel}} u}}{\sigma_y}, \frac{\sqrt{2P_{\mathrm{sel}} z}}{\sigma_y}\right)\right)^{K-1} dz dv du\right)\Bigg] dx, \end{aligned} \tag{24}$$

where $Q_1(\cdot,\cdot)$ is the Marcum-Q function and $I_0(\cdot)$ is the zeroth-order modified Bessel function of the first kind [34, Ch. 5].

Proof: The proof is given in Appendix E. ∎

To the best of our knowledge, the above integral cannot be simplified further. It is more involved than the expression in (12) due to the aforementioned correlated Rician RVs. However, considerable insight can be gleaned from the high and low SNR asymptotic regimes, and from a novel upper bound that we derive below. The exact expression helps us

Authorized licensed use limited to: Indian Institute of Technology. Downloaded on February 05,2025 at 11:59:49 UTC from IEEE Xplore. Restrictions apply.

verify the accuracy of the asymptotic analysis and the tightness of the upper bound.

Lemma 2: For $(P_{\text{sel}}/\sigma^2) \to \infty$ and large K, we have

$$B_{\text{g}} \to \frac{5}{4}\beta_r\gamma + \beta_d + \sqrt{\pi\beta_d\beta_r \log(K)} + \beta_r \log(K) - \frac{\beta_r}{4}\log\left(\frac{16\pi^2\beta_d}{\beta_r}\log(K)\right). \quad (25)$$

Proof: The proof is given in Appendix F. ∎

Similar to (22), this corresponds to a genie-aided selection of the reflection pattern. Its dominant term grows logarithmically with K and linearly with β_d.

As $(P_{\text{sel}}/\sigma^2) \to 0$, we can show that

$$B_{\text{g}} \to \beta_{\text{eff}} \triangleq \beta_d + \beta_r. \quad (26)$$

Similar to (23), this is equal to the beamforming gain of a random-phase configuration. This special case was derived in [29].

Upper Bound: To capture the dependence of B_{g} on P_{sel}, which the above asymptotic analysis does not bring out, we derive an upper bound that holds for small and large P_{sel}, i.e., when $(P_{\text{sel}}/\sigma^2) \to 0$ and $(P_{\text{sel}}/\sigma^2) \to \infty$. To do that, we introduce new i.i.d. RVs $z(1), z(2), \ldots, z(K) \sim \mathcal{CN}(0, \beta_d)$ that are independent of h_d and $\mathbf{r}$. Consider the following virtual selection criterion that selects the reflection pattern $\boldsymbol{\phi}(u)$, where

$$u = \text{argmax}_{i\in\{1,2,\ldots,K\}} \left|\sqrt{P_{\text{sel}}}\left(z(i) + \mathbf{r}^T\boldsymbol{\phi}(i)\right) + n_i\right|^2. \quad (27)$$

We call this a virtual criterion since it replaces h_d with $z(1), \ldots, z(K)$. It is only introduced for analysis. It is not implemented in practice. As the following result shows, it provides an insightful, tractable bound on the beamforming gain of the proposed scheme.

Theorem 3: For small and large P_{sel}, the beamforming gain $\mathbb{E}\left[|h_{eq}(u)|^2\right]$ of the virtual selection criterion in (27) upper bounds the beamforming gain $\mathbb{E}\left[|h_{eq}(s)|^2\right]$ of the selected reflection pattern.

Proof: The proof is given in Appendix G. ∎

Notice that $z(i) + \mathbf{r}^T\boldsymbol{\phi}(i) \sim \mathcal{CN}(0, \beta_d + \beta_r)$, $\forall i \in \{1, 2, \ldots, K\}$. Using this fact and simplifying along lines similar to Appendices B and C, we can show that

$$\mathbb{E}\left[|h_{eq}(u)|^2\right] = \frac{\beta_{\text{eff}}\left(P_{\text{sel}}\beta_{\text{eff}}\left[\psi(K+1)+\gamma\right] + \sigma^2\right)}{P_{\text{sel}}\beta_{\text{eff}} + \sigma^2}. \quad (28)$$

Furthermore, from Theorem 3, $\mathbb{E}\left[|h_{eq}(s)|^2\right] \le \mathbb{E}\left[|h_{eq}(u)|^2\right]$.

The numerical results in Section V indicate that the above bound holds for any P_{sel}, even though we proved it only for small and large values of P_{sel}. Furthermore, the bound is tight in the sense that it becomes an equality when the direct link weakens, i.e., $\beta_d \to 0$. This is because the beamforming gain expression in (28) simplifies to that in (12).

B. Achievable Rate and Its Optimization

When the direct link is present, we apply the selection-aware estimator in (11), except that we use the expression in (28) for $\mathbb{E}\left[|h_{eq}(s)|^2\right]$.

Along lines similar to Section III-B, it follows that the upper bound on the achievable rate in (17), which depends on B_{g}, applies to this case also. Given the tractable form of the upper bound in (28), we use it in (17) instead of the exact multi-integral expression for B_{g}.

Substituting (28) for B_{g} in (21), the corresponding objective function $\eta(P_c, P_{\text{sel}})$ is given by

$$\eta(P_c, P_{\text{sel}}) = \frac{\left(P_T - KP_{\text{sel}} - P_c\right)P_c}{\sigma^2\left(P_{\text{sel}}\beta_d + \sigma_y^2\right)} \times \frac{\left(\beta_{\text{eff}} f\left(P_{\text{sel}}\right)\right)^2}{\left(\begin{array}{c}\left(P_T - KP_{\text{sel}} + (\tau_d - 1)P_c\right)\beta_{\text{eff}} f\left(P_{\text{sel}}\right) \\ + \left(P_{\text{sel}}\beta_d + \sigma_y^2\right)\tau_d\sigma^2\end{array}\right)}, \quad (29)$$

where $f\left(P_{\text{sel}}\right) = P_{\text{sel}}\beta_{\text{eff}}\left[\psi(K+1)+\gamma\right] + \sigma^2$.

We see that the term β_r in (21), which is derived for the scenario in which the direct link is blocked, is replaced by $\beta_d + \beta_r$. The optimal powers are determined by numerically maximizing the above expression, subject to the constraints in (19) and (20). This is done in a manner similar to that in Section III-C. We do not repeat the steps here due to space constraints.

V. Numerical Results and Discussions

We now present numerical results to quantify the impact of power allocation and overheads on the achievable rate. Unless mentioned otherwise, the number of IRS elements M is 128 and the coherence interval duration T_{c} is 400 symbols. The IRS element width and height are equal to the carrier's wavelength. The path-loss model is as follows: $\beta_g = \beta_0(d_g/d_0)^{-\alpha_g}$, $\beta_h = \beta_0(d_h/d_0)^{-\alpha_h}$, where $d_0 = 1$ m is the reference distance, $\beta_0 = -20$ dB is the path-loss at the reference distance, d_g is the distance between the AP and the IRS, d_h is the distance between the IRS and the user, and $\alpha_g = 2$ and $\alpha_h = 2.1$ are the path-loss exponents of the AP-IRS and IRS-user channels, respectively [4], [29]. We set $d_g = 5$ m and $d_h = 40$ m, which imply that $\beta_g = -34$ dB and $\beta_h = -54$ dB. The noise variance is $\sigma^2 = -103.6$ dBm. We set $\tau_f = \tau_c = 1$. The achievable rate in (13) is determined by averaging over $10,000$ fade realizations. We shall refer to $P_T\beta_r/(T_{\text{c}}\sigma^2)$ as the SNR. We first show the results for independent IRS channel gains and then for correlated IRS channel gains.

First, we assess the efficacy of the selection-aware estimator. For this, we compare its normalized MSE $\mathbb{E}\left[|h_{eq}(s) - \hat{h}_{eq}(s)|^2\right] \Big/ \mathbb{E}\left[|h_{eq}(s)|^2\right]$ with the normalized MSE of the selection-unaware estimator. Figure 2 plots the normalized MSE as a function of the demodulation pilot SNR $P_c\beta_r/\sigma^2$ for the scenarios without and with the direct link. The MSE decreases as the pilot SNR increases. We see that the analysis and simulation results for the proposed estimator

Authorized licensed use limited to: Indian Institute of Technology. Downloaded on February 05,2025 at 11:59:49 UTC from IEEE Xplore. Restrictions apply.

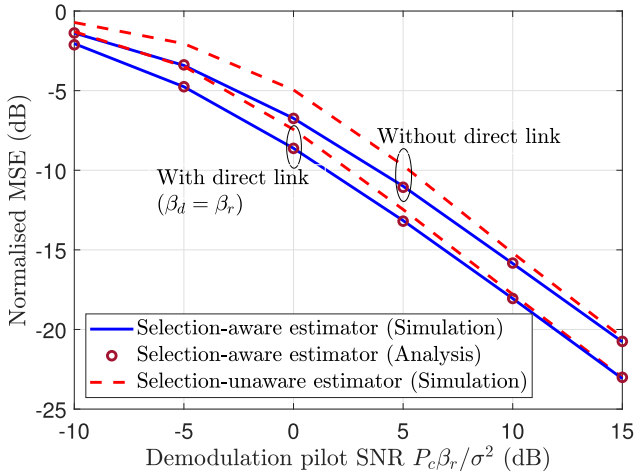


Fig. 2. Normalized MSE as a function of the demodulation pilot SNR $P_c\beta_r/\sigma^2$ with and without direct link ($P_{\text{sel}}\beta_r/\sigma^2 = 15$ dB and $K = 25$).

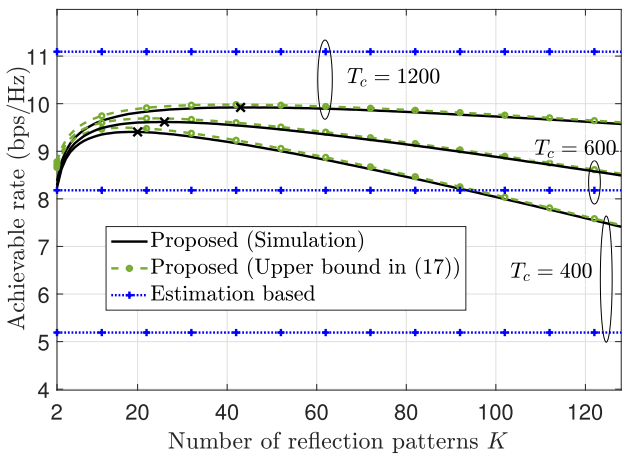


Fig. 3. Achievable rate as a function of the number of reflection patterns (K) for different channel coherence times ($P_T = 15$ dBm). The maximum rate is shown by the marker '×'.

match each other well. Furthermore, the MSE with the direct link is lower than the MSE without the direct link. At low pilot SNRs, the MSE of the selection-aware estimator is lower than that of the selection-unaware estimator. The gap between the two estimators decreases as the pilot SNR increases.

We benchmark the proposed scheme with the following:

1) *Equal Power Allocation (EPA) Scheme*: Here, the same power is allocated to each selection pilot, demodulation pilot, and data symbol. The reflection pattern s with the largest received signal strength is selected as per (4). Furthermore, the unordered statistics of the beamforming gain are used to estimate $h_{eq}(s)$. The training and feedback overhead is $K + 2\tau_f + \tau_c + 1$, which is the same as that of the proposed scheme.
2) *Instantaneous CSI-based Scheme [2], [3], [5], [6]*: Here, the user sends M pilots to the AP with the columns of the DFT matrix as the reflection patterns at the IRS. Then, the AP estimates the cascaded IRS channel gains, determines the phase-shifts of IRS elements, and conveys them to the IRS via a control link. Thus, the training and feedback overhead is equal to $M + M\tau_c + \tau_f + 1$.[3] The same power is allocated to each selection pilot, demodulation pilot, and data symbol. This DFT-based scheme is known to outperform the on-off scheme of [3] and [4].
3) *Random Phase-Shift Scheme [3], [5], [6]*: Here, a random phase-shift is configured at each IRS element. Hence, no selection pilots are required; one demodulation pilot suffices. Thus, the training and feedback overhead is $\tau_f + 1$. The same power is allocated to the demodulation pilot and each data symbol.
4) *Genie-Aided Scheme*: Here, the selection of reflection pattern is assumed to be noise-free. Thus, $s = \text{argmax}_{1\le i\le K}\left\{|h_{eq}(i)|^2\right\}$. Furthermore, $h_{eq}(s)$ is assumed to be known perfectly to the AP and the user. The training and feedback overhead is 0.

[3]Here, the control overhead is $M\tau_c$ since the reflection coefficients of M elements have to be sent via the control link.

A. Without Direct Link

Figure 3 plots the achievable rate and its upper bound in (17) as a function of the codebook size K, which is also equal to the number of selection pilots, for different T_c. As K increases, the achievable rate initially increases. This is due to an increase in the beamforming gain, as shown in Corollary 2. However, for larger K, the rate decreases. This is because the increase in the training overhead negates the rate gains due to the increase in the beamforming gain. This shows the trade-off between the rate and the precision of the K codewords. For $T_c = 400$, 600, and 1200, we see that $K = 20$, 26, and 43, respectively, are optimal. Thus, the optimal codebook size increases as the T_c increases. We see that the upper bound is tight for all values of K and T_c. We, therefore, do not distinguish between the two henceforth. The rate achieved by the estimation-based scheme is also shown. It is smaller than that of the codebook-based scheme except at large T_c. When T_c is large, the fraction of time spent on training by the estimation-based scheme is small. In this regime, the beamforming gain of the estimation-based scheme is proportional to M^2 [29]. On the other hand, the beamforming gain of the codebook-based scheme is proportional to $M\psi(K+1)$ (by Corollary 1).

Figure 4 plots the achievable rate as a function of the demodulation pilot power SNR $P_c\beta_g\beta_h/\sigma^2$ for different values of the selection pilot SNR $P_{\text{sel}}\beta_g\beta_h/\sigma^2$. The rate initially increases as P_c increases due to an increase in the accuracy of the channel estimates. On the other hand, for large P_c, the rate decreases as P_c increases because of lesser power for data. As P_{sel} increases, the rate increases because of the increase in the beamforming gain (by Corollary 2). However, for large P_{sel}, the rate decreases because less power is available for the demodulation pilot and the data. The optimal value of P_c, which maximizes the rate, is shown using the marker ×. It is insensitive to P_{sel}.

Figure 5 plots the achievable rate as a function of the SNR. The rate increases as the SNR increases for all schemes. We compare with the genie-aided scheme, which assumes perfect channel estimates and no training overhead. Therefore,

Authorized licensed use limited to: Indian Institute of Technology. Downloaded on February 05,2025 at 11:59:49 UTC from IEEE Xplore. Restrictions apply.

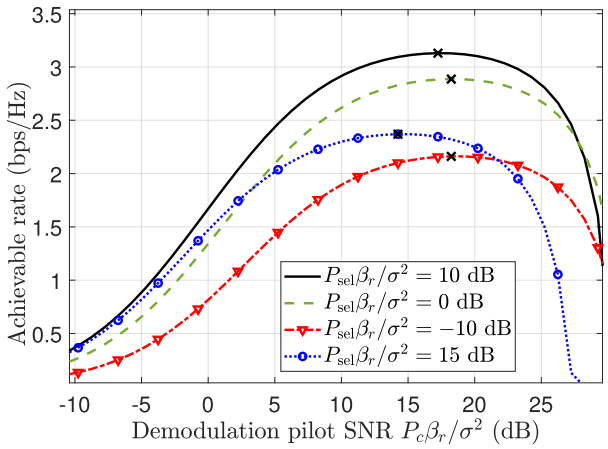


Fig. 4. Achievable rate as a function of the demodulation pilot SNR $P_c\beta_r/\sigma^2$ for different values of selection pilot SNR $P_{\text{sel}}\beta_r/\sigma^2$ ($K = 25$ and SNR $= 5$ dB). The maximum rate is shown by the marker '$\times$'.

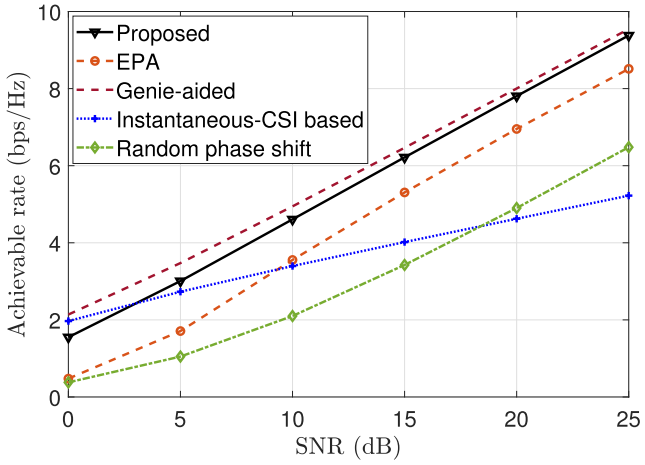
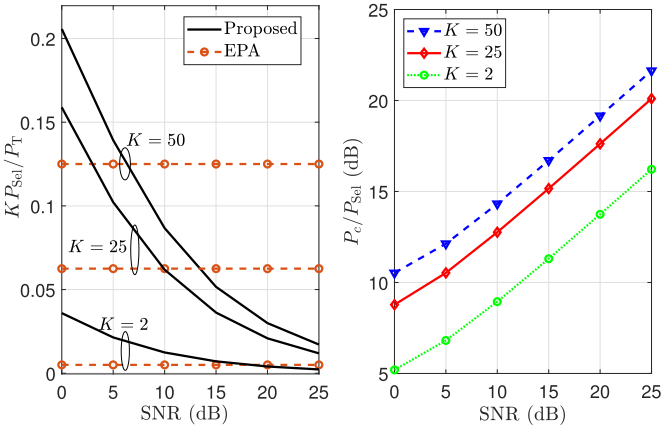


Fig. 5. Performance benchmarking: Achievable rate as a function of the SNR for optimal power allocation, EPA, estimation-based, genie-aided, and random phase-shift schemes ($K = 25$).

it serves as an upper limit for any other scheme. We see that the proposed optimal scheme performs close to that of the genie-aided scheme and the gap decreases as the SNR increases. Therefore, it is competitive with any other scheme. It also achieves a higher rate than the EPA and random phase-shift schemes for all SNRs. At low SNRs, the instantaneous-CSI based scheme performs marginally better than optimal power allocation due to its larger beamforming gain. However, at high SNRs, the large training overheads of the estimation-based scheme cause its rate to be lower than even the random phase-shift scheme.

Figure 6(a) plots the ratio of the optimal total selection pilots power (KP_{sel}) to the total power as a function of the SNR for different values of K. Also shown are results for the EPA scheme, for which this ratio is equal to the constant $\frac{K}{P_T}\frac{P_T}{T_c} = \frac{K}{T_c}$. For the optimal power allocation, the ratio decreases for all K as the SNR increases. At low SNRs, relatively more power gets allocated to the selection pilots to improve the odds that the optimal reflection pattern is selected. On the other hand, at high SNRs, more power is set aside for the demodulation pilot and the data. In this regime, the power



(a) Selection pilots' power (b) Demodulation pilot power

Fig. 6. Ratio of demodulation pilot and selection pilot powers as a function of the SNR for different K.

allocated to the selection pilots is less than that allocated by the EPA scheme. As K increases, more power gets allocated to the K selection pilots.

Figure 6(b) plots the corresponding ratio (in dB) of the optimal demodulation and selection pilot powers as a function of the SNR for different values of K. For the EPA scheme, this ratio is always equal to 0 dB. Notably, the optimal scheme allocates significantly more power to the demodulation pilot than the selection pilot, unlike EPA. As the SNR or K increases, the ratio increases.

B. Impact of Correlated Cascaded Channel Gains

We now study the case where the IRS-user channel gains are correlated due to close spacing of the IRS elements. The correlation coefficient $C_{i,j}$ of h_i and h_j for an isotropic scattering environment is given by [33]

$$C_{i,j} = \text{sinc}\left(\frac{2||u_i - u_j||}{\lambda}\right), \text{ for } i,j \in \{1,2,\ldots,M\}, \quad (30)$$

where u_i is the location of the i^{th} element, $||.||$ denotes distance, and λ is the wavelength. The elements are arranged in a 16×8 uniform planar array, with the horizontal and vertical inter-element distances being d. The power allocation of the proposed scheme is as per Section III-C.

Figure 7 plots the achievable rate as a function of the wavelength-normalized length d/λ for the proposed, EPA, and genie-aided schemes. The random phase-shift and estimation-based schemes, which perform worse, are not shown to avoid clutter. As d/λ increases, the effective area of the IRS also increases. This leads to an increase in the beamforming gain and rate [33]. The proposed power allocation achieves a higher rate than EPA at both high and low SNRs. Its rate is close to that of the genie-aided scheme, and the gap between the two decreases as the SNR increases.

C. With Direct Link

Figure 8 plots the achievable rate of the optimal power allocation scheme and its upper bound (from Theorem 3) as a function of M for different relative strengths $\beta_d/(\beta_g\beta_h)$

Authorized licensed use limited to: Indian Institute of Technology. Downloaded on February 05,2025 at 11:59:49 UTC from IEEE Xplore. Restrictions apply.

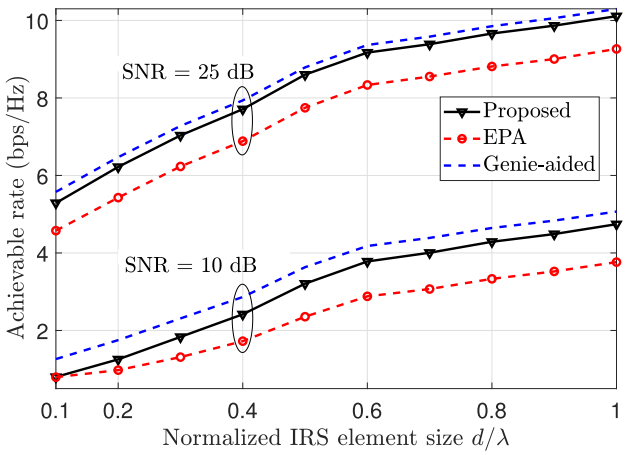
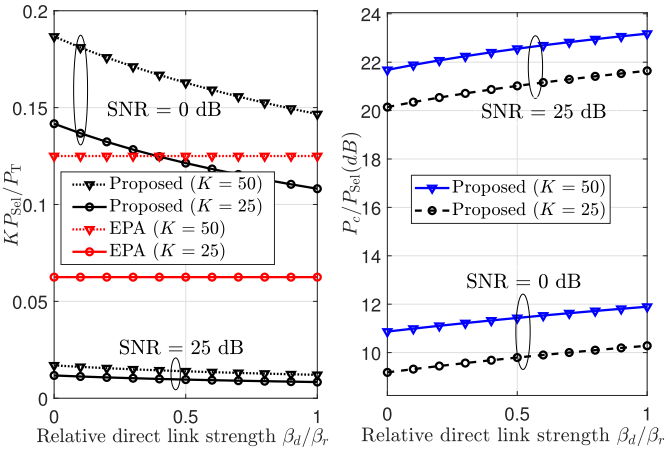


Fig. 7. Correlated channel fading: Achievable rates as a function of the normalized IRS element size (uniform planar array with 16×8 elements and $K = 25$).



(a) Ratio of selection pilot power to total power (b) Ratio of demodulation and selection pilot powers

Fig. 9. With direct link: Pilot power allocation as a function of the relative direct link strength β_d/β_r for different K and SNRs.

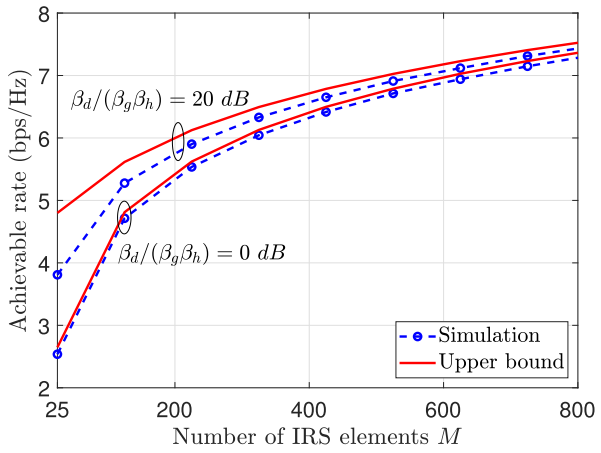


Fig. 8. With direct link: Achievable rate and the upper bound (Theorem 3) of the optimal power allocation scheme as a function of M for different values of $\beta_d/(\beta_g\beta_h)$ ($K = 25$ and $P_T = 0$ dBm).

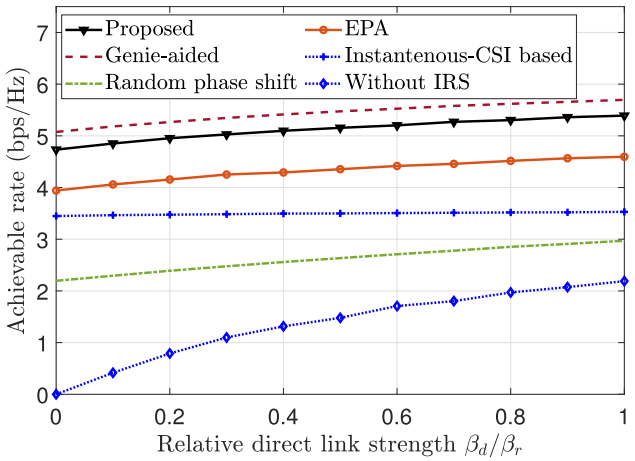


Fig. 10. Performance benchmarking: Achievable rate as a function of β_d/β_r for the proposed, EPA, genie-aided, estimation based and random phase-shift schemes, and a non-IRS system ($P_T = 0$ dBm and $K = 25$).

of the direct link compared to the cascaded links. The upper bound becomes tighter as the relative strength of the direct link decreases. This is because the virtual selection rule, which is used to derive the bound, becomes the same as the actual selection rule in the absence of direct link. Furthermore, the bound becomes tight as M increases. The rate increases as M increases or as the relative strength of the direct link increases. The slope of the curve decreases as M increases because the rate is a logarithmic function of M.

Figure 9(a) shows the ratio KP_{sel}/P_T of the total selection pilot power to the total power available as a function of β_d/β_r for the proposed and EPA schemes at SNRs of 0 dB and 25 dB. For EPA, the ratio is equal to K/T_c, and is not a function of β_d/β_r. As β_d/β_r increases, the optimal ratio decreases for all K. This is because the IRS contributes less to the overall SNR and the rate as the direct link becomes stronger. Therefore, the proposed scheme allocates more power to the data symbols and less to the selection pilots. As before, the proposed scheme allocates more power to the selection pilots than the EPA scheme at low SNRs, while the reverse is true at high SNRs. Figure 9(b) plots the corresponding ratio of the powers of the demodulation and selection pilots P_c/P_{sel}. The proposed scheme again allocates more power to the demodulation pilot than the selection pilot. Furthermore, the ratio of these pilot powers is larger compared to the scenario where the direct link is blocked.

Figure 10 compares the achievable rate of the proposed, EPA, genie-aided, DFT-based estimation, and random phase-shift schemes for $K = 25$. Also shown is the rate achieved by a non-IRS system. As the ratio β_d/β_r increases, the rate increases for all the schemes. The rate achieved by the DFT-based estimation scheme increases at a slower rate than that of the proposed scheme as β_d increases, since it suffers from a large pilot and control signaling overhead. The proposed scheme achieves a higher rate than all the other schemes and is close to the genie-aided scheme. Its rate is at least 2.4 times higher than that of the non-IRS system over the entire range of β_d/β_r.

Authorized licensed use limited to: Indian Institute of Technology. Downloaded on February 05,2025 at 11:59:49 UTC from IEEE Xplore. Restrictions apply.

VI. Conclusion

For the codebook-based training scheme, noise affected the choice of the IRS reflection pattern and the estimate of the effective channel gain used for coherently demodulating the data. We proposed a novel selection-aware LMMSE estimator to estimate the effective channel gain. When the direct link was blocked, we derived a closed-form expression of the IRS beamforming gain and a tight bound on the achievable rate that accounted for the cumulative impact of the channel estimation errors and the training, feedback, and control signaling overheads. When both direct and reflected links were present, we derived tight bounds for the beamforming gain and the achievable rate. The optimal powers allocated to the selection and demodulation pilots and data were different, with substantially more power being allocated to the demodulation pilot than a selection pilot. The optimal codebook size increased as the coherence interval increased. Our proposed approach achieved a higher rate than the estimation-based scheme except when $M \ll T_{\mathrm{c}}$. The same conclusions held when the cascaded channel gains were correlated due to closely-spaced IRS elements.

Several avenues for future work exist. These include considering hierarchical or non-orthogonal codebooks and modeling frequency-selective channels. Extending our analysis to multiple antennas at the AP and the users is another open problem. In this case, the impact of the channel estimation errors on the precoding vector at the AP also needs to be characterized.

Appendix

A. Proof of Lemma 1

We know that the g_m is a deterministic channel gain with $|g_m|^2 = \beta_g$ and $h_1, \ldots, h_M$ are i.i.d. $\mathcal{CN}(0, \beta_h)$. Therefore, $r_1 = h_1 g_1, r_2 = h_2 g_2, \ldots, r_M = h_M g_M$ are i.i.d. complex normal RVs with mean 0 and variance $\beta_g \beta_h$, and $\mathbf{r}$ is a complex normal random vector, i.e., $\mathbf{r} \sim \mathcal{CN}(\mathbf{0}, \beta_g \beta_h \mathbf{I}_M)$.

The effective channel gains $h_{eq}(1) = \mathbf{r}^T \boldsymbol{\phi}(1), h_{eq}(2) = \mathbf{r}^T \boldsymbol{\phi}(2), \ldots, h_{eq}(K) = \mathbf{r}^T \boldsymbol{\phi}(K)$ are the projections of $\mathbf{r}$ onto the orthogonal codebook vectors $\boldsymbol{\phi}(1), \boldsymbol{\phi}(2), \ldots, \boldsymbol{\phi}(K)$. Thus, $h_{eq}(1), h_{eq}(2), \ldots, h_{eq}(K)$ are i.i.d. complex normal RVs with mean 0 and variance $M \beta_g \beta_h$ [35, Ch. 2.2.4].

B. Proof of Theorem 1

Let $h_{eq}(m) = e_{rm} + j e_{im}$, for $m \in \{1, 2, \ldots, K\}$. The cumulative distribution function (CDF) $F_{h_{eq}(s)}(.)$ of $h_{eq}(s)$ in terms of its real and imaginary parts is given by

$$F_{h_{eq}(s)}(x + jz) \triangleq F_{e_{rs}, e_{is}}(x, z) = \Pr\left(e_{rs} \leq x, e_{is} \leq z\right). \tag{31}$$

Since the events $s = 1, s = 2, \ldots, s = K$ are mutually exclusive, we have

$$F_{h_{eq}(s)}(x + jz) = \sum_{m=1}^{K} \Pr\left(e_{rs} \leq x, e_{is} \leq z, s = m\right). \tag{32}$$

Since all reflection patterns are equally likely, we have

$$F_{h_{eq}(s)}(x + jz) = K \Pr\left(e_{r1} \leq x, e_{i1} \leq z, s = 1\right). \tag{33}$$

Let $\mathcal{K}_1 = \{2, 3, \ldots, K\}$. From (4), we know that $s = 1$, when $|y_1|^2 > |y_2|^2, \ldots, |y_1|^2 > |y_K|^2$. Therefore,

$$F_{h_{eq}(s)}(x + jz) = K \Pr\left(e_{r1} \leq x, e_{i1} \leq z, |y_1|^2 > |y_m|^2, \forall m \in \mathcal{K}_1\right). \tag{34}$$

Conditioning on e_{r1} and e_{i1} and then averaging over them, we get

$$F_{h_{eq}(s)}(x + jz) = K\, \mathbb{E}\left[\mathbb{1}_{\{e_{r1} \leq x, e_{i1} \leq z,\}} \times \Pr\left(|y_m|^2 < |y_1|^2, \forall m \in \mathcal{K}_1 | e_{r1}, e_{i1}\right)\right]. \tag{35}$$

From Lemma 1, we know that $y_2, y_3, \ldots, y_K$ are independent of e_{r1} and e_{i1}. Furthermore, $y_m \sim \mathcal{CN}(0, \sigma_y^2)$, $\forall m \in \mathcal{K}_1$. Hence, $|y_m|^2$, $\forall m \in \mathcal{K}_1$, are i.i.d. exponential RVs with mean σ_y^2. Therefore, the probability term in (35) when conditioned on $|y_1|^2$ is given by

$$\Pr\left(|y_m|^2 < |y_1|^2, \forall m \in \mathcal{K}_1 | e_{r1}, e_{i1}, |y_1|^2\right) = \left(1 - \exp\left(-|y_1|^2/\sigma_y^2\right)\right)^{K-1}. \tag{36}$$

After averaging over $|y_1|^2$, we get

$$\Pr\left(|y_m|^2 < |y_1|^2, \forall m \in \mathcal{K}_1 | e_{r1}, e_{i1}\right) = \mathbb{E}\left[\left(1 - \exp\left(-|y_1|^2/\sigma_y^2\right)\right)^{K-1}\right]. \tag{37}$$

Given e_{r1} and e_{i1}, we have $y_1 \sim \mathcal{CN}(\sqrt{P_{\mathrm{sel}}}(e_{r1} + j e_{i1}), \sigma^2)$. Therefore, $|y_1|^2$ given e_{r1} and e_{i1} is a non-central chi-square RV with conditional PDF given by

$$\frac{1}{\sigma^2} \exp\left(-\frac{w + P_{\mathrm{sel}} e_{a1}^2}{\sigma^2}\right) I_0\left(\sqrt{\frac{4 P_{\mathrm{sel}} e_{a1}^2 w}{\sigma^4}}\right), w \geq 0, \tag{38}$$

where $e_{a1}^2 = e_{r1}^2 + e_{i1}^2$ and $I_0(\cdot)$ is the zeroth-order modified Bessel function of the first kind [34, Ch. 5]. Using this conditional PDF in (37), we get

$$\Pr\left(|y_m|^2 < |y_1|^2, \forall m \in \mathcal{K}_1 | e_{r1}, e_{i1}\right) = \frac{1}{\sigma^2} \int_0^{\infty} \left(1 - \exp\left(-w/\sigma_y^2\right)\right)^{K-1} \exp\left(-\frac{w + P_{\mathrm{sel}} e_{a1}^2}{\sigma^2}\right) \times I_0\left(\sqrt{\frac{4 P_{\mathrm{sel}} e_{a1}^2 w}{\sigma^4}}\right) dw. \tag{39}$$

Using the binomial expansion [36], we get

$$\Pr\left(|y_m|^2 < |y_1|^2, \forall m \in \mathcal{K}_1 | e_{r1}, e_{i1}\right) = \frac{1}{\sigma^2} e^{-\frac{P_{\mathrm{sel}} e_{a1}^2}{\sigma^2}} \sum_{l=0}^{K-1} \left[\binom{K-1}{l} (-1)^l \times \int_0^{\infty} e^{-\frac{w}{\sigma^2} - \frac{w l}{\sigma_y^2}} I_0\left(\sqrt{\frac{4 P_{\mathrm{sel}} e_{a1}^2 w}{\sigma^4}}\right) dw\right]. \tag{40}$$

Using the identities in [37, (2) and (9)], the above probability term simplifies to

$$\Pr\left(|y_m|^2 < |y_1|^2, \forall m \in \mathcal{K}_1 | e_{r1}, e_{i1}\right) = \sum_{l=0}^{K-1} \binom{K-1}{l} \frac{(-1)^l \sigma_y^2}{(l+1)(\sigma_y^2 + l\sigma^2)} e^{-\frac{P_{\mathrm{sel}} l e_{a1}^2}{\sigma_y^2 + l\sigma^2}}. \tag{41}$$

Authorized licensed use limited to: Indian Institute of Technology. Downloaded on February 05,2025 at 11:59:49 UTC from IEEE Xplore. Restrictions apply.

Substituting (41) in (35) and evaluating the expectation over e_{r1} and e_{i1}, we get

$$F_{e_{rs},e_{is}}(x,z) = \frac{K}{\pi\beta_r}\sum_{l=0}^{K-1}\binom{K-1}{l}(-1)^l\frac{\sigma_y^2}{\sigma_y^2+l\sigma^2} \times \int_{-\infty}^{z}\int_{-\infty}^{x}\exp\left(-\frac{(l+1)(e_{r1}^2+e_{i1}^2)\sigma_y^2}{\beta_r(\sigma_y^2+l\sigma^2)}\right) de_{r1}\, de_{i1}. \quad (42)$$

Simplifying the above double integral using [36, (2.33)], we get the following expression for the CDF of $h_{eq}(s)$:

$$F_{e_{rs},e_{is}}(x,z) = \frac{K}{4}\sum_{l=0}^{K-1}\binom{K-1}{l}\frac{(-1)^l}{(l+1)} \times\left[1+\text{erf}\left(\sqrt{\frac{(l+1)\sigma_y^2}{\beta_r(\sigma_y^2+l\sigma^2)}}x\right)\right] \times\left[1+\text{erf}\left(\sqrt{\frac{(l+1)\sigma_y^2}{\beta_r(\sigma_y^2+l\sigma^2)}}z\right)\right], \quad (43)$$

where erf is the error function [36, (8.250)]. Partially differentiating (43) with respect to x and z yields (10).

C. Brief Proof of Corollary 1

Using the PDF of $h_{eq}(s)$ in (10), we can show that the PDF of $|h_{eq}(s)|^2$ is given by

$$f_{|h_{eq}(s)|^2}(x) = \frac{K\sigma_y^2}{\beta_r}\sum_{l=0}^{K-1}\binom{K-1}{l}\frac{(-1)^l}{(\sigma_y^2+l\sigma^2)} \times\exp\left(\frac{-(l+1)\sigma_y^2}{(\sigma_y^2+l\sigma^2)\beta_r}x\right),\ x\geq 0. \quad (44)$$

We can show that the first moment of this PDF is given by

$$\mathbb{E}\left[|h_{eq}(s)|^2\right] = \frac{K\beta_r}{\sigma_y^2}\sum_{l=0}^{K-1}\binom{K-1}{l}\frac{(-1)^l\left(\sigma_y^2+l\sigma^2\right)}{(l+1)^2}. \quad (45)$$

Using the identities in [36, (8.365) and (8.367)] yields (12).

D. Proof of Corollary 2

Using the properties of the digamma function, it can be shown that (12) is a monotonically increasing function of K. It is easy to show that (12) is a monotonically increasing function of P_{sel}.

To prove concavity, we differentiate (12) twice with respect to P_{sel}. Doing so yields

$$\frac{\partial^2\,\mathbb{E}\left[|h_{eq}(s)|^2\right]}{\partial^2 P_{\text{sel}}} = -\frac{2\beta_r^3\sigma^2\left[\psi^{(0)}(K+1)+\gamma-1\right]}{\sigma_y^6}. \quad (46)$$

The above quantity is negative since $\sigma_y^2>0$ and $\psi^{(0)}(K+1)+\gamma-1>0$ for $K>1$ [31, Ch. 6]. Hence, $\mathbb{E}\left[|h_{eq}(s)|^2\right]$ is concave in P_{sel}.

Differentiating (12) twice with respect to K, which we treat as a real number, we get

$$\frac{\partial^2\,\mathbb{E}\left[|h_{eq}(s)|^2\right]}{\partial^2 K} = \frac{P_{\text{sel}}\beta_r^2\psi^{(2)}(K+1)}{\sigma_y^2}, \quad (47)$$

where $\psi^{(2)}(.)$ is the second derivative of the digamma function. The second derivative in (47) is negative since $\psi^{(2)}(K+1)<0$ for $K\geq 1$ [31, Ch. 6] and $\mathbb{E}\left[|h_{eq}(s)|^2\right]$ is concave in K.

E. Proof of Theorem 2

Let $\omega_i=\mathbf{r}^T\boldsymbol{\phi}(i)$. Thus, $h_{eq}(i)=\omega_i+h_d$, for $1\leq i\leq K$. From Appendix A, we know that $\omega_1,\omega_2,\ldots,\omega_K$ are i.i.d. and $\omega_i\sim\mathcal{CN}(0,\beta_r)$.

Similar to (35), the CDF of $|h_{eq}(s)|^2$ can be written as

$$F_{|h_{eq}(s)|^2}(x) = K\,\mathbb{E}\left[\mathbb{1}_{\{|h_{eq}(1)|^2\leq x\}} \times\Pr\left(|y_m|^2<|y_1|^2,\forall m\in\mathcal{K}_1|h_{eq}(1),h_d\right)\right], \quad (48)$$

where the conditioning is on both $h_{eq}(1)$ and h_d.

To evaluate $\Pr\left(|y_m|^2<|y_1|^2,\forall m\in\mathcal{K}_1|h_{eq}(1),h_d\right)$, we first obtain the probability of $|y_m|^2<|y_1|^2,\forall m\in\mathcal{K}_1$, given $h_{eq}(1)$, h_d, and $|y_1|^2$. Conditioned on h_d, we know that y_i, $\forall i\in\mathcal{K}_1$, are i.i.d. non-central complex normal RVs with $y_i\sim\mathcal{CN}(\sqrt{P_{\text{sel}}}h_d,\beta_r+\sigma^2)$. Furthermore, given $|y_1|^2$, we know that: (i) the events $|y_m|^2<|y_1|^2$, $\forall m\in\mathcal{K}_1$, are independent, and (ii) $|y_m|^2$, $\forall m\in\mathcal{K}_1$, are independent non-central chi-square RVs. Using [34, Ch. 5], we can then show that

$$\Pr\left(|y_m|^2<|y_1|^2,\forall m\in\mathcal{K}_1|h_{eq}(1),h_d,|y_1|^2\right) = \left(1-Q_1\left(\frac{\sqrt{2P_{\text{sel}}|h_d|^2}}{\sigma_y},\frac{\sqrt{2P_{\text{sel}}|y_1|^2}}{\sigma_y}\right)\right)^{K-1}, \quad (49)$$

where Q_1 is the Marcum-Q function.

Conditioned on $h_{eq}(1)$ and h_d, $y_1\sim\mathcal{CN}(\sqrt{P_{\text{sel}}}h_{eq}(1),\sigma^2)$. Thus, the PDF of $|y_1|^2$ conditioned on $h_{eq}(1)$ and h_d is obtained by replacing e_{a1}^2 in (38) with $|h_{eq}(1)|^2$. Using this conditional PDF, we get

$$\Pr\left(|y_m|^2<|y_1|^2,\forall m\in\mathcal{K}_1|h_{eq}(1),h_d\right) = \frac{1}{\sigma^2}\int_0^\infty\left(1-Q_1\left(\frac{\sqrt{2P_{\text{sel}}|h_d|^2}}{\sigma_y},\frac{\sqrt{2P_{\text{sel}}z}}{\sigma_y}\right)\right)^{K-1} \times I_0\left(\sqrt{\frac{4P_{\text{sel}}|h_{eq}(1)|^2z}{\sigma^4}}\right)e^{\frac{-\left(z+P_{\text{sel}}|h_{eq}(1)|^2\right)}{\sigma^2}}dz. \quad (50)$$

Substituting this in (48) and taking the expectation over $h_{eq}(1)$ and h_d, we get

$$F_{|h_{eq}(s)|^2}(x) = \frac{1}{\beta_r\beta_d\sigma^2}\int_0^\infty\int_0^x\int_0^\infty e^{-\frac{u+v}{\beta_r}}e^{-\frac{u}{\beta_d}} \times I_0\left(\sqrt{\frac{4uv}{\beta_r^2}}\right)I_0\left(\sqrt{\frac{4P_{\text{sel}}vz}{\sigma^4}}\right)e^{\frac{-(z+P_{\text{sel}}v)}{\sigma^2}} \times\left(1-Q_1\left(\frac{\sqrt{2P_{\text{sel}}u}}{\sigma_y},\frac{\sqrt{2P_{\text{sel}}z}}{\sigma_y}\right)\right)^{K-1}dzdvdu. \quad (51)$$

Authorized licensed use limited to: Indian Institute of Technology. Downloaded on February 05,2025 at 11:59:49 UTC from IEEE Xplore. Restrictions apply.

Substituting the above CDF in the formula $\mathbb{E}\left[|h_{eq}(s)|^2\right] = \int_0^\infty \left(1 - F_{|h_{eq}(s)|^2}(x)\right) dx$ yields (24).

F. Proof of Lemma 2

Let

$$Z = \max_{1\le i\le K} \left\{|h_{eq}(i)|^2\right\}. \tag{52}$$

When $(P_{\text{sel}}/\sigma^2) \to \infty$, the noise term in (2) becomes negligible. Thus, $|h_{eq}(s)|^2 = Z$. From the law of total expectation, we have

$$\mathbb{E}\left[|h_{eq}(s)|^2\right] = \mathbb{E}_{h_d}\left[\mathbb{E}_{Z|h_d}[Z]\right]. \tag{53}$$

$|h_d|^2$ is an exponential RV with mean β_d. Substituting this in (53), we get

$$\mathbb{E}\left[|h_{eq}(s)|^2\right] = \frac{1}{\beta_d}\int_0^\infty \mathbb{E}_{Z|h_d}[Z] \exp\left(\frac{-x}{\beta_d}\right) dx. \tag{54}$$

Conditioned on h_d, $|h_{eq}(i)|^2$ is a non-central chi-square RV with shape parameters v and σ', $\forall i \in \{1, 2, \ldots, K\}$, where $v = |h_d|$ and $2\sigma'^2 = \beta_r$ [38]. Let

$$b_K = \beta_r\left[\log(K) - \frac{1}{4}\log\left(\log(K)\right) + 2|h_d|\sqrt{\frac{\log(K)}{\beta_r}} - \frac{1}{2}\log\left(\frac{4\pi|h_d|}{\sqrt{\beta_r}} e^{\frac{-2|h_d|^2}{\beta_r}}\right)\right]. \tag{55}$$

By extreme value theory, for large K, $\frac{Z-b_K}{\beta_r}$ follows the standard Gumbel distribution with CDF equal to $\exp(-\exp(-z))$, for $z > 0$ [38]. Therefore, $\mathbb{E}_{Z|h_d}[Z] = \gamma M\beta_g\beta_h + b_K$. Substituting b_k from (55), we get

$$\mathbb{E}_{Z\big|h_d}[Z] = \beta_r\gamma + \beta_r\log(K) + 2|h_d|\sqrt{\beta_r\log(K)} - \frac{\beta_r}{4}\log\left(\frac{16\pi^2|h_d|^2}{\beta_r} e^{\frac{-4|h_d|^2}{\beta_r}}\log(K)\right). \tag{56}$$

Substituting (56) in (54) and using the identities in [36, (3.381) and (4.331)] yields (25).

G. Proof of Theorem 3

We now derive this for large P_{sel} (i.e., $(P_{\text{sel}}/\sigma^2) \to \infty$) and small P_{sel} (i.e., $(P_{\text{sel}}/\sigma^2) \to 0$) separately.

a) When $(P_{sel}/\sigma^2) \to \infty$: Here, the noise term is negligible and the selection in (4) simplifies to

$$s = \text{argmax}_{i\in\{1,2,\ldots,K\}} \left|h_d + \mathbf{r}^T\boldsymbol{\phi}(i)\right|^2. \tag{57}$$

By construction, we know that $z(i)$ used in the virtual selection criterion in (27) is independent of s. Therefore, where $x \overset{p}{\sim} y$ denotes that x and y obey the same statistics.

Let Υ denote the maximum value of the sequence

$$\left|z(1) + \mathbf{r}^T\boldsymbol{\phi}(1)\right|^2, \left|z(2) + \mathbf{r}^T\boldsymbol{\phi}(2)\right|^2, \ldots \ldots, \left|z(s-1) + \mathbf{r}^T\boldsymbol{\phi}(s-1)\right|^2, \left|h_d + \mathbf{r}^T\boldsymbol{\phi}(s)\right|^2, \left|z(s+1) + \mathbf{r}^T\boldsymbol{\phi}(s+1)\right|^2, \ldots, \left|z(K) + \mathbf{r}^T\boldsymbol{\phi}(K)\right|^2, \tag{58}$$

where $z(s)$ has been replaced by h_d in the s^{th} term. Since $z(s) \overset{p}{\sim} h_d$, we know that $\Upsilon \overset{p}{\sim} \left|z(u) + \mathbf{r}^T\boldsymbol{\phi}(u)\right|^2$, which implies $\mathbb{E}[\Upsilon] = \mathbb{E}\left[\left|z(u) + \mathbf{r}^T\boldsymbol{\phi}(u)\right|^2\right] = \mathbb{E}\left[|h_{eq}(u)|^2\right]$.

From the definition of Υ, we can say that $\Upsilon \ge \left|h_d + \mathbf{r}^T\boldsymbol{\phi}(s)\right|^2$. Thus, $\mathbb{E}[\Upsilon] \ge \mathbb{E}\left[\left|h_d + \mathbf{r}^T\boldsymbol{\phi}(s)\right|^2\right]$, which implies that

$$\mathbb{E}\left[|h_{eq}(u)|^2\right] = \mathbb{E}\left[\left|z(u) + \mathbf{r}^T\boldsymbol{\phi}(u)\right|^2\right] \ge \mathbb{E}\left[\left|h_d + \mathbf{r}^T\boldsymbol{\phi}(s)\right|^2\right] = \mathbb{E}\left[|h_{eq}(s)|^2\right]. \tag{59}$$

b) When $(P_{sel}/\sigma^2) \to 0$: From (27), we know that $|h_{eq}(u)|^2 \ge \left|z(1) + \mathbf{r}^T\boldsymbol{\phi}(1)\right|^2$. Since h_d and $z(1)$ are i.i.d., we get $\left|z(1) + \mathbf{r}^T\boldsymbol{\phi}(1)\right|^2 \overset{p}{\sim} \left|h_d + \mathbf{r}^T\boldsymbol{\phi}(1)\right|^2$. These together imply that

$$\mathbb{E}\left[|h_{eq}(u)|^2\right] = \mathbb{E}\left[\left|h_d + \mathbf{r}^T\boldsymbol{\phi}(u)\right|^2\right] \ge \mathbb{E}\left[|h_{eq}(1)|^2\right]. \tag{60}$$

When $(P_{\text{sel}}/\sigma^2) \to 0$, it follows from (4) that $s = \text{argmax}_{1\le i\le K}\left\{|n_i|^2\right\}$. Thus, s is independent of h_d and $\mathbf{r}$. In such a case, $|h_{eq}(s)| \overset{p}{\sim} |h_{eq}(1)|$ and $\mathbb{E}\left[|h_{eq}(s)|^2\right] = \mathbb{E}\left[|h_{eq}(1)|^2\right]$. Combining this with (60) yields the bound in (59). The expression for $\mathbb{E}\left[\left|h_d(u) + \mathbf{r}^T\boldsymbol{\phi}(u)\right|^2\right]$ is the same as that in (28).

REFERENCES

[1] S. Ganesan, N. B. Mehta, and R. Sarvendranath, "A novel demodulation and selection pilot power trade-off for codebook-based IRS with imperfect channel estimates," in *Proc. IEEE Int. Conf. Acoust., Speech Signal Process. (ICASSP)*, Apr. 2024, pp. 8876–8880.

[2] E. Basar, M. Di Renzo, J. de Rosny, M. Debbah, M.-S. Alouini, and R. Zhang, "Wireless communications through reconfigurable intelligent surfaces," *IEEE Access*, vol. 7, pp. 116753–116773, 2019.

[3] Y. Yang, B. Zheng, S. Zhang, and R. Zhang, "Intelligent reflecting surface meets OFDM: Protocol design and rate maximization," *IEEE Trans. Commun.*, vol. 68, no. 7, pp. 4522–4535, Jul. 2020.

[4] J. An, L. Wang, C. Xu, L. Gan, and L. Hanzo, "Optimal pilot power based channel estimation improves the throughput of intelligent reflective surface assisted systems," *IEEE Trans. Veh. Technol.*, vol. 69, no. 12, pp. 16202–16206, Dec. 2020.

[5] B. Zheng and R. Zhang, "Intelligent reflecting surface-enhanced OFDM: Channel estimation and reflection optimization," *IEEE Wireless Commun. Lett.*, vol. 9, no. 4, pp. 518–522, Apr. 2020.

[6] C. You, B. Zheng, and R. Zhang, "Channel estimation and passive beamforming for intelligent reflecting surface: Discrete phase shift and progressive refinement," *IEEE J. Sel. Areas Commun.*, vol. 38, no. 11, pp. 2604–2620, Nov. 2020.

[7] S. Naduvilpattu and N. B. Mehta, "Optimal time and power allocation for phase-shift configuration and downlink channel estimation in RIS-aided systems," *IEEE Trans. Wireless Commun.*, vol. 23, no. 8, pp. 9419–9431, Aug. 2024.

[8] Z. Wang, L. Liu, and S. Cui, "Channel estimation for intelligent reflecting surface assisted multiuser communications: Framework, algorithms, and analysis," *IEEE Trans. Wireless Commun.*, vol. 19, no. 10, pp. 6607–6620, Oct. 2020.

[9] P. Cai, J. Zong, X. Luo, Y. Zhou, S. Chen, and H. Qian, "Downlink channel tracking for intelligent reflecting surface-aided FDD MIMO systems," *IEEE Trans. Veh. Technol.*, vol. 70, no. 4, pp. 3341–3353, Apr. 2021.

[10] D. Shen and L. Dai, "Dimension reduced channel feedback for reconfigurable intelligent surface aided wireless communications," *IEEE Trans. Commun.*, vol. 69, no. 11, pp. 7748–7760, Nov. 2021.

[11] N. K. Kundu, Z. Li, J. Rao, S. Shen, M. R. McKay, and R. Murch, "Optimal grouping strategy for reconfigurable intelligent surface assisted wireless communications," *IEEE Wireless Commun. Lett.*, vol. 11, no. 5, pp. 1082–1086, May 2022.

Authorized licensed use limited to: Indian Institute of Technology. Downloaded on February 05,2025 at 11:59:49 UTC from IEEE Xplore. Restrictions apply.

[12] A. Taha, M. Alrabeiah, and A. Alkhateeb, "Enabling large intelligent surfaces with compressive sensing and deep learning," *IEEE Access*, vol. 9, pp. 44304–44321, 2021.
[13] Ö. Özdogan and E. Björnson, "Deep learning-based phase reconfiguration for intelligent reflecting surfaces," in *Proc. 54th Asilomar Conf. Signals, Syst., Comput.*, Pacific Grove, CA, USA, Nov. 2020, pp. 707–711.
[14] Y. Jin et al., "Multiple residual dense networks for reconfigurable intelligent surfaces cascaded channel estimation," *IEEE Trans. Veh. Technol.*, vol. 71, no. 2, pp. 2134–2139, Feb. 2022.
[15] L. Dai and X. Wei, "Distributed machine learning based downlink channel estimation for RIS assisted wireless communications," *IEEE Trans. Commun.*, vol. 70, no. 7, pp. 4900–4909, Jul. 2022.
[16] X. Zhu, W. Chen, Q. Wu, and L. Wang, "Performance analysis of RIS-aided space shift keying with channel estimation errors," in *Proc. IEEE/CIC Int. Conf. Commun. China (ICCC)*, Aug. 2023, pp. 1–6.
[17] K. Zhi et al., "Two-timescale design for reconfigurable intelligent surface-aided massive MIMO systems with imperfect CSI," *IEEE Trans. Inf. Theory*, vol. 69, no. 5, pp. 3001–3033, May 2023.
[18] K. Zhi, C. Pan, H. Ren, and K. Wang, "Power scaling law analysis and phase shift optimization of RIS-aided massive MIMO systems with statistical CSI," *IEEE Trans. Commun.*, vol. 70, no. 5, pp. 3558–3574, May 2022.
[19] K. Zhi, C. Pan, G. Zhou, H. Ren, M. Elkashlan, and R. Schober, "Is RIS-aided massive MIMO promising with ZF detectors and imperfect CSI?" *IEEE J. Sel. Areas Commun.*, vol. 40, no. 10, pp. 3010–3026, Oct. 2022.
[20] J. An, C. Xu, L. Wang, Y. Liu, L. Gan, and L. Hanzo, "Joint training of the superimposed direct and reflected links in reconfigurable intelligent surface assisted multiuser communications," *IEEE Trans. Green Commun. Netw.*, vol. 6, no. 2, pp. 739–754, Jun. 2022.
[21] J. An, C. Xu, L. Gan, and L. Hanzo, "Low-complexity channel estimation and passive beamforming for RIS-assisted MIMO systems relying on discrete phase shifts," *IEEE Trans. Commun.*, vol. 70, no. 2, pp. 1245–1260, Feb. 2022.
[22] A. M. Nor, O. Fratu, and S. Halunga, "Positioning information-based codebook for reconfigurable intelligent surface passive beamforming," *IEEE Open J. Commun. Soc.*, vol. 4, pp. 3115–3130, 2023.
[23] J. An et al., "Codebook-based solutions for reconfigurable intelligent surfaces and their open challenges," *IEEE Wireless Commun.*, vol. 31, no. 2, pp. 134–141, Apr. 2024.
[24] Y. Zhang, B. Di, H. Zhang, M. Dong, L. Yang, and L. Song, "Dual codebook design for intelligent omni-surface aided communications," *IEEE Trans. Commun.*, vol. 21, no. 11, pp. 9232–9245, Nov. 2022.
[25] S. Zhang, Y. Zhang, H. Zhang, N. Ye, and B. Di, "Rate-overhead tradeoff for IOS-aided beam training: How large codebook is enough for the IOS?" *IEEE Wireless Commun. Lett.*, vol. 12, no. 6, pp. 1081–1085, Jun. 2023.
[26] J. Wang, W. Tang, S. Jin, C.-K. Wen, X. Li, and X. Hou, "Hierarchical codebook-based beam training for RIS-assisted mmWave communication systems," *IEEE Trans. Commun.*, vol. 71, no. 6, pp. 3650–3662, Jun. 2023.
[27] P. Wang, J. Fang, W. Zhang, and H. Li, "Fast beam training and alignment for IRS-assisted millimeter wave/terahertz systems," *IEEE Trans. Wireless Commun.*, vol. 21, no. 4, pp. 2710–2724, Apr. 2022.
[28] V. Jamali, M. Najafi, R. Schober, and H. V. Poor, "Power efficiency, overhead, and complexity tradeoff of IRS codebook design—Quadratic phase-shift profile," *IEEE Commun. Lett.*, vol. 25, no. 6, pp. 2048–2052, Jun. 2021.
[29] Q. Wu and R. Zhang, "Intelligent reflecting surface enhanced wireless network via joint active and passive beamforming," *IEEE Trans. Wireless Commun.*, vol. 18, no. 11, pp. 5394–5409, Nov. 2019.
[30] S. M. Kay, *Fundamentals of Statistical Signal Processing: Estimation Theory*, 1st ed., Upper Saddle River, NJ, USA: Prentice-Hall, 1993.
[31] M. Abramowitz and I. A. Stegun, *Handbook of Mathematical Functions: With Formulas, Graphs, and Mathematical Tables*, 1st ed., New York, NY, USA: Dover, 1965.
[32] B. Hassibi and B. M. Hochwald, "How much training is needed in multiple-antenna wireless links?" *IEEE Trans. Inf. Theory*, vol. 49, no. 4, pp. 951–963, Apr. 2003.
[33] E. Björnson and L. Sanguinetti, "Rayleigh fading modeling and channel hardening for reconfigurable intelligent surfaces," *IEEE Wireless Commun. Lett.*, vol. 10, no. 4, pp. 830–834, Apr. 2021.
[34] A. F. Molisch, *Wireless Communications*, 2nd ed., Hoboken, NJ, USA: Wiley, 2011.
[35] D. Tse and P. Viswanath, *Fundamentals of Wireless Communication*, 1st ed., Cambridge, U.K.: Cambridge Univ. Press, 2005.
[36] I. S. Gradshteyn and I. M. Ryzhik, *Table of Integrals, Series, and Products*, 7th ed. Amsterdam, The Netherlands: Elsevier, 2007.
[37] A. H. Nuttall, *Some Integrals Involving the Q-Function*. Fort Belvoir, VA, USA: Defense Technical Information Center, 1972.
[38] A. Subhash, S. Kalyani, Y. H. Al-Badarneh, and M.-S. Alouini, "On the asymptotic performance analysis of the k-th best link selection over non-identical non-central chi-square fading channels," *IEEE Trans. Commun.*, vol. 70, no. 11, pp. 7191–7206, Nov. 2022.



Sriram Ganesan received the B.E. degree in electronics and communication engineering from the Thiagarajar College of Engineering, Madurai, in 2021, and the M.Tech. degree in electronics and communication engineering from the Indian Institute of Science, Bengaluru, in 2023. He is currently a Wireless Research and Development Systems Engineer with Qualcomm. His research interests include wireless communication, signal processing, and algorithm design and development for next generation technologies.



Neelesh B. Mehta (Fellow, IEEE) received the B.Tech. degree in electronics and communications engineering from the Indian Institute of Technology (IIT) Madras in 1996 and the M.S. and Ph.D. degrees in electrical engineering from California Institute of Technology, Pasadena, USA, in 1997 and 2001, respectively. He is currently a Professor and the Chair of the Department of Electrical Communication Engineering, Indian Institute of Science, Bengaluru. He is a fellow of the Indian National Science Academy, the Indian Academy of Sciences, the Indian National Academy of Engineering, and the National Academy of Sciences India. He was a recipient of the J. C. Bose Fellowship, the Shanti Swarup Bhatnagar Award, the Khosla Award, the Vikram Sarabhai Research Award, and the Swarnajayanti Fellowship. He served on the Board of Governors for the IEEE ComSoc, from 2012 to 2015. He serves on ComSoc's Nominations and Elections Committee. He served on the Executive Editorial Committee for IEEE TRANSACTIONS ON WIRELESS COMMUNICATIONS from 2014 to 2017 and the Chair from 2017 to 2018. He has served as an Editor for IEEE TRANSACTIONS ON COMMUNICATIONS and IEEE WIRELESS COMMUNICATION LETTERS in the past.



Rimalapudi Sarvendranath (Member, IEEE) received the B.Tech. degree in electrical and electronics engineering from the National Institute of Technology Karnataka, Surathkal, India, in 2009, and the M.E. and Ph.D. degrees from the Department of Electrical Communication Engineering, Indian Institute of Science (IISc), Bengaluru, India, in 2012 and 2020, respectively. He is currently an Assistant Professor with the Department of Electrical Engineering, Indian Institute of Technology (IIT) Tirupati, Tirupati, India. In 2021, he was a Post-Doctoral Researcher with the Department of Electrical Engineering, Linköping University, Linköping, Sweden. He was an Assistant Professor with the Department of Electronics and Electrical Engineering, IIT Guwahati, from January 2022 to June 2023. From 2012 to 2016, he was with Broadcom Communications Technologies, Bengaluru, where he worked on developing and implementing algorithms for LTE and IEEE 802.11ac wireless standards. He received the Kaikini Research Fellowship in 2017, granted to one student among all engineering departments at IISc. He received the Innovation in Science Pursuit for Inspired Research (INSPIRE) Faculty Fellowship in 2022. His research interests include machine learning for wireless communication, multiple antenna techniques, spectrum sharing, and next-generation wireless standards.

Authorized licensed use limited to: Indian Institute of Technology. Downloaded on February 05,2025 at 11:59:49 UTC from IEEE Xplore. Restrictions apply.